# LARGE EDDY SIMULATIONS OF COMPLEX TURBULENT FLOWS USING IMMERSED BOUNDARY METHOD

MAYANK TYAGI, SUMANTA ACHARYA
*Mechanical Engineering Department*
*Louisiana State University, Baton Rouge, LA*

## Abstract

Large eddy simulations (LES) are performed for two representative complex geometry problems of particular interest to turbomachinery flows. First problem studied is the flow field inside a trapped-vortex combustor. Second problem is the unsteady interaction of rotor blade with stator blade wake field. The representation of complex geometry is done using immersed boundary method (IBM). Two different implementations are presented for the body force terms.

## 1. Introduction

Simulation of turbulent flows in complex geometries is a daunting task. LES can formally alleviate the issue of ever-increasing resolution demand for high Reynolds number flow. However, complex geometries pose the problem of commutation errors on curvilinear grids. Moreover, the representation of moving geometries using either sliding meshes or regenerating the mesh becomes overwhelmingly complicated in complex situations. IBM relies upon the body force terms added in the momentum equations to represent the geometry on a fixed Cartesian mesh (Peskin, 1977, Mohd.-Yusof, 1996, Glowinski et al., 1994, Fadlun et al. 2000, Kellog, 2000). This formulation is simple and ideally suited for the moving geometries involving no-slip walls with prescribed trajectories and locations.

## 2. Governing Equations

In the immersed boundary method, the complex geometrical features are incorporated by adding a forcing function in the governing equations. The forcing function is zero everywhere except at the surface where the influence of the solid boundaries is assigned (Subscript Γ).

$$\frac{\tilde{u}-u^n}{\Delta t}=\frac{3}{2}\left(C^n+D^n\right)-\frac{1}{2}\left(C^{n-1}+D^{n-1}\right)+f$$

$$f=[\frac{u_\Gamma^{n+1}-u^n}{\Delta t}-\frac{3}{2}\left(C^n+D^n\right)+\frac{1}{2}\left(C^{n-1}+D^{n-1}\right)]\delta(\vec{x}-\vec{x}_\Gamma)$$

$$\frac{u^{n+1}-\tilde{u}}{\Delta t}=-\nabla p^{n+1}$$

where the convective terms are represented by $C$ and the diffusion terms are represented by $D$. In case of highly refined meshes, it may be necessary to treat some directions implicitly for diffusion terms (generally using Crank-Nicholson scheme).

$$C = -(u \cdot \nabla)u, D = \frac{1}{\mathrm{Re}} \nabla^2 u$$

To obtain the pressure Poisson equation, take the divergence of the second step and enforce the continuity condition for the velocity field at the next time step

$$\nabla^2 p = \frac{\nabla \cdot \tilde{u}}{\Delta t} - \nabla \cdot f - \frac{\nabla \cdot u^{n+1}}{\Delta t}$$

$$\because \nabla \cdot u^{n+1} = 0$$

$$\Rightarrow \nabla^2 p = \frac{\nabla \cdot \tilde{u}}{\Delta t} - \nabla \cdot f$$

Therefore, the Poisson equation for pressure can be solved prior to the second step in the time-split scheme. The spatial discretization is performed using fourth order central difference schemes. For the two problems studied, two different implementations for the body force terms are presented. The trapped-vortex combustor is a complicated but stationary geometry and hence, interpolation on only one-side of the geometry is adequate. However, for moving rotor blade the interpolation is performed on both sides of the curved surface.

CASE A: *Forcing at only one side of the immersed boundary (inside the virtual solid)*

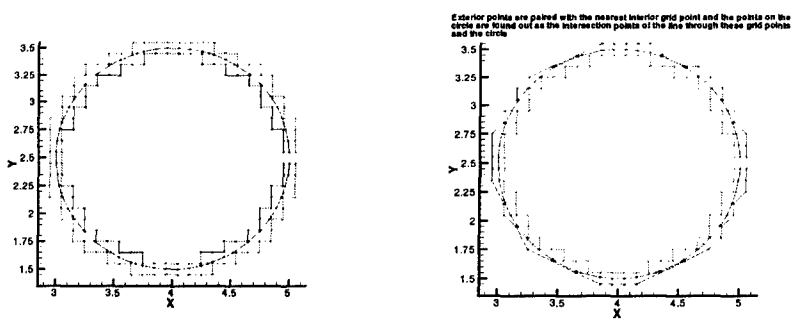


Figure 1 Identification of the circular boundary on uniform 2-D cartesian mesh and evaluation of the nearest exterior point corresponding to each identified interior point

Let $\Delta$ be the mesh spacing and $\delta$ be the distance of the forcing point from the immersed surface. Therefore, we apply the linear interpolation/extrapolation among the forced point, point on the immersed surface and the point just outside the virtual solid. Let $V_d$ be the desired velocity at the point on the immersed

surface and $V_c$ be the computed velocity in the region of interest. Therefore, the velocity at the forcing point $V_{im}$ is given by

$$[V_c - V_d]/[\Delta - \delta] = [V_d - V_{im}]/[\delta]$$
$$V_{im} = V_d\,[\Delta]/[\Delta - \delta] - V_c\,[\delta]/[\Delta - \delta]$$

Clearly, In the limit $\delta$ going to zero, i.e. the forcing point approaching the point on the immersed surface, we retrieve the limit $V_{im}$ approaching $V_d$. However, In the limit $\delta$ approaching mesh spacing $\Delta$, we have $V_c$ approaching $V_d$. $V_{im}$ is ill-defined because it is the difference between $V_d$ and $V_c$ with very large coefficients. For such coefficients, $V_c$ is set equal to $V_d$.

CASE B: *Forcing at both sides of the immersed boundary (inside the virtual solid and at the very first point outside the virtual solid)*

Let $\Delta$ be the mesh spacing and $\delta$ be the distance of the forcing point from the immersed surface. Therefore, we apply the linear interpolation/extrapolation among the forced points, point on the immersed surface and the computed point just outside the virtual solid (Figure 2). Let $V_d$ be the desired velocity at the point on the immersed surface and $V_c$ be the computed velocity in the region of interest. Therefore, the velocity at the internal forcing point $V_{int}$ is given by

$$[V_c - V_d]/[2\Delta - \delta] = [V_d - V_{int}]/[\delta]$$
$$V_{int} = V_d\,[2\Delta]/[2\Delta - \delta] - V_c\,[\delta]/[2\Delta - \delta]$$

Similarily, the velocity at the external forcing point $V_{ext}$ is given by

$$[V_c - V_d]/[2\Delta - \delta] = [V_{ext} - V_d]/[\Delta - \delta]$$
$$V_{ext} = V_d\,[\Delta]/[2\Delta - \delta] + V_c\,[\Delta - \delta]]/[2\Delta - \delta]$$

Clearly, in the limit $\delta$ going to zero, i.e. the internal forcing point approaching the point on the immersed surface, we retrieve the limit $V_{int}$ approaching $V_d$ and $V_{ext}$ approaching $[V_d + V_c]/2$. Moreover, In the limit $\delta$ approaching mesh spacing $\Delta$, we have $V_{ext}$ approaching $V_d$ . $V_{int}$ is defined as $[2V_d - V_c]$ as it should be by reflection condition. Thus, the forcing remains physical for all positions of the immersed surface between the grid interfaces. For moving boundary implementation, it will be important for another reason. It avoids reflected velocities to show up in the region of interest.

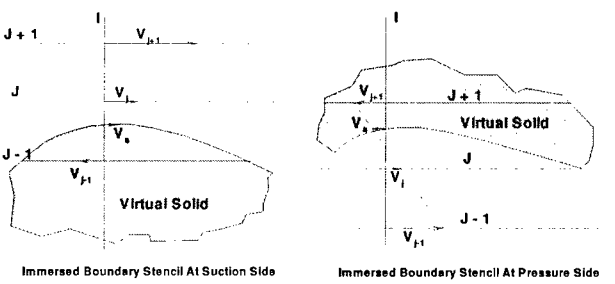


Figure 2 Identification of the interpolation stencils for a moving rotor blade.

## 3. Trapped Vortex Combustor

### 3.1 Problem Description

A uniform cartesian grid of 92×57×117 points is used for a domain containing the upper half of the TV combustor. All the dimensions are selected to approximate the experimental setup of Mancilla (2001) within Cartesian geometry. Ratio of air injection velocity to the mainflow velocity is 2.2. Reynolds number based on the annular mainflow velocity and air hole dimension (D) is 3400 for these simulations. The radii of the forebody, the connecting tube, the afterbody and the outer shell are 24.5D, 3.7D, 23D and 27.5D respectively. The lengths of the forebody, the connecting tube and the afterbody are 12D, 30D and 12D respectively. The periodicity of the geometry is exploited by putting half of the jet injections around the bottom of the computational domain with the boundary conditions obtained by the rotational symmetry about the axial direction. At the inflow, fully developed laminar profile along with fluctuations is prescribed. The fluctuations are assumed to be Gaussian and are calculated using Box-Muller algorithm. At the walls, no slip boundary conditions are imposed using immersed boundary method. Uniform injections of air and fuel are applied at the respective holes on the afterbody. Periodic boundary conditions are applied in the spanwise (z) direction. At the outflow, a non-reflective convective scheme is applied to convect away the flow structures out of the computational domain without any spurious reflections. The wave speed is calculated to maintain the mass flux balance in the whole domain.

### 3.2 Results

The three-dimensional simulations showed that the vorticity magnitude of the trapped vortex in the cavity changes due to vortex stretching mechanism that is absent in the two-dimensional simulations done by other researchers (Katta and Roquomore, 1996 and Stone and Menon, 2000). The motion of the trapped vortex is unsteady inside the cavity as observed experimentally as well as numerically (Mancilla, 2001). Unsteady dynamics of the coherent structures inside the cavity is a slower process as compared to the separation region over the afterbody and the mixing layer region behind the forebody lip. The ingestion of annular mainflow in front of the afterbody separation region is the main mechanism of the flow entrainment inside the cavity. The mixture in the cavity is ejected radially outwards due to the pressure gradients there. The instantaneous axial and radial locations of the TV are different at different meridional planes. However, time-averaged streamtrace patterns seem to converge towards a TV with simpler geometrical features.

#### TIME AVERAGED FLOW FIELD

The streamtraces are presented at the meridional planes $\theta = 90°$, $0°$ and $180°$ (figure 3). At $\theta = 90°$, the large recirculation region is formed between the annular mainflow and the fuel injections. The unsteadiness of the mixing layer

and the motion of TV inside the cavity has been averaged out. At $\theta = 0°$ and 180°, the streamtraces are asymmetric implying that a longer averaging period is needed to completely eliminate the slow variations. Moreover, the axisymmetry is also absent at these meridional planes. The TV is a doughnut shaped structure inside the cavity. The pitch of the spiral formed by streamtraces close to the meridional plane $\theta = 90°$ is largest. The azimuthal motion of the streamtraces along the surface of the TV is absent in all the previous 2-D studies. However, the core of the TV is mostly irrotational.

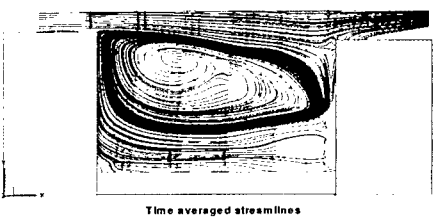


(a)

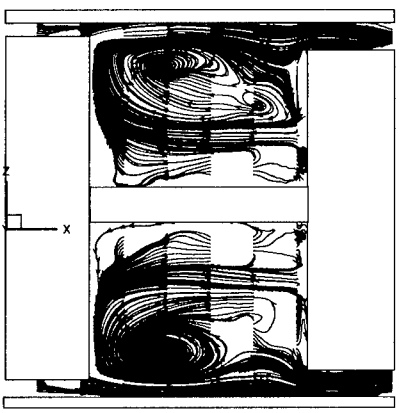


(b)

Figure 3 Streamtraces at (a) $\theta = 90°$ (b) $\theta = 0°$ and 180° (tracers are released along radial positions at several axial locations).

TURBULENT STRESSES (No Figures)

At $\theta = 90°$, the turbulent shear stress $u'v'$ inside the cavity is mostly generated by the production terms ($u'u'.\partial V/\partial x$ and $v'v'.\partial U/\partial y$) around the mixing layer region. The high axial momentum fluctuations of the fluid parcels are correlated with radially inward fluctuations around the mixing layer region. This implies the turbulent mixing and diffusion is enhanced between the cavity and annular mainflow by this stress component. The shear stress is also large along the jet injections. However, the levels of turbulent stresses indicate that flow is mostly laminar close to the forebody and connecting tube junction. At $\theta = 0°$ and 180°, the turbulent shear stress $u'w'$ inside the cavity is mostly generated by the production terms ($u'u'.\partial W/\partial x$ and $w'w'.\partial U/\partial z$) around the jets in the cavity and the mixing layer region. This distribution indicates enhanced mixing of fluid parcels inside the core of TV. The distribution of $u'w'$ near the jet injections is dictates the radial spread of the jets along the axial direction in the cavity. At X/D = 40.8, the radial fluctuations are high at different azimuthal or meridional planes. The normal stress $u'u'$ is mostly negligible due to suppression

of fluctuations normal to the face of the afterbody. The only significant levels are above the afterbody in the annular region. The distribution of the shear stress $v'w'$ along the jets is primarily due to turbulent production ($v'v'.\partial W/\partial y$ and $w'w'.\partial V/\partial z$). The distribution in the annular region seems to attain the periodicity between the fuel injections. It can be expected that the modeling of the shear stress tensor components using an eddy viscosity approximation may work here since the shear stress components depend on the corresponding mean strain rate tensor components only.

## 4. Unsteady Stator-Rotor Interactions

### 4.1 Problem Description

The inherent unsteadiness of a turbomachinery flow field created by relative motion between stationary blades (stator) and the rotating blades (rotor), requires the designer to account for three-dimensional as well as unsteady effects. The unsteadiness is caused by (a) the interaction of the rotor airfoils with the wakes and passage vortices generated by upstream airfoils, (b) the relative motion of the rotors with respect to the stators (potential effect), and (c) the shedding of vortices by the airfoils because of the blunt trailing edges (Rai and Madavan, 1990, Saxer and Giles, 1994). Computation of such flows is complicated by relative motion between rotor and stator airfoils and the periodic transition of the flow from laminar to turbulent. Unsteady simulations have been performed using multitudes of approximations such as unsteady RANS, "average-passage" approach and "mixing-plane" approach. These calculations have been performed invariably using "sliding mesh" techniques requiring further modeling of "apparent stresses" and "phase-lagged" interface conditions (Sharma et al., 1994). In the present study, we utilize LES with moving IBM to simulate unsteady stator-rotor interactions. Though, the calculation is performed for incompressible fluid at a low Reynolds number, it demonstrates the strength of the method by avoiding all ad-hoc assumptions pertaining to RANS modeling and sliding meshes. A uniform Cartesian grid of 302×202×11 points is used for a domain of the size 3D×1D×0.1D, where D is the chord length of the rotor airfoil. Choice of a small spanwise dimension may not allow larger physical scales and hence may not be desirable. The geometry of the airfoils is taken from the numerical study of Kelecy et al (1995). The airfoil profile is approximated by the cubic spline surfaces. The airfoil is divided into leading edge, trailing edge, pressure surface and suction surface to ensure that immersed boundary conditions are enforced on enough grid points to realize the geometry. Uniform flow field is specified at the inflow. Periodic boundary conditions are applied in the direction of rotor motion (y) and the spanwise (z) direction. Reynolds number base on the inflow velocity and rotor chord length is 5000. At the outflow, a non-reflective convective scheme is applied to convect away the flow structures out of the computational domain without any spurious reflections. The wave speed is calculated to maintain the mass flux balance in the whole domain.

4.2 Results

Four snapshots of the instantaneous vorticity field are shown in figure 4 at time instants T apart (=0.12$\tau$, where $\tau$ is the non-dimensional time scale). There is a separation region on the suction side of the stator. The trailing edge vortices of the stator blade impact on the suction side of the rotor blade near its leading edge. The trailing edge vortices of the rotor and the vortices formed due to the interaction of stator wake and suction-side boundary layer are shed into the passage flow and convected out of the domain.

a) $t_0$

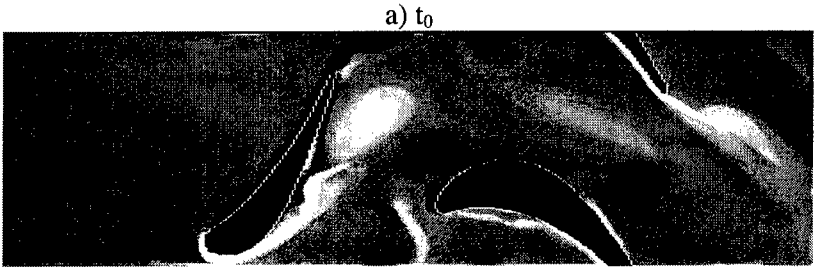

b) $t_0 + T$

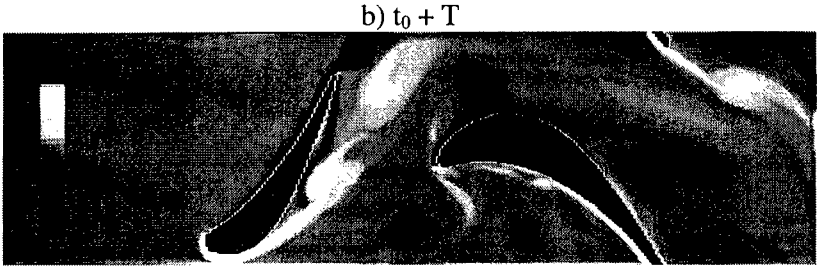

c) $t_0 + 2T$

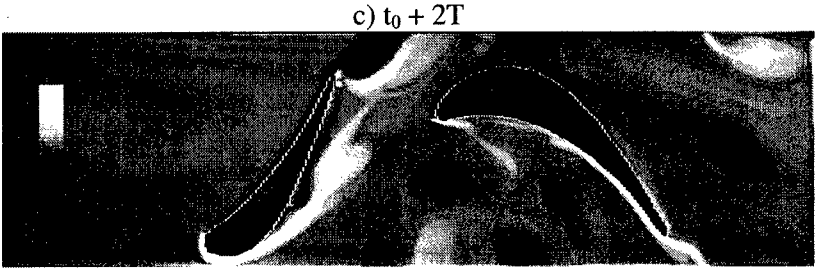

d) $t_0 + 3T$

Figure 4 Instantaneous snapshots of vorticity component at time a) $t = t_0$, b) $t = t_0+T$, c) $t = t_0+2T$ and d) $t = t_0+3T$.

## 5. Concluding Remarks

The merit of immersed boundary method (IBM) for simulating moving complex geometries on Cartesian mesh has been demonstrated. High order of accuracy of discretization schemes is retained which is very important for LES. The problems studied are a) Trapped vortex combustor (TVC) and b) Stator-rotor interactions in a transonic turbine stage. In TVC case study, mixing inside an annular cavity is analyzed. In stator-rotor case study, the superiority of this method is demonstrated over existing methodologies such as sliding meshes. Moreover, the ad-hoc modeling for the "apparent stresses" is not needed in the realms of LES. In future, a zonal refinement treatment of the immersed boundaries will be implemented to capture the essential near wall physics to render this method with predictive capabilities.

## References

Fadlun, E., Verzicco, R., Orlandi, P. and Yusof, J. M. (2000), Combined immersed-boundary finite-difference methods for three-dimensional complex flow simulations, *J. Comp. Phy.*, Vol. 161, pp. 35-60.

Glowinski, R., Pan, T.-W. and Periaux, J. (1994), A ficitious domain method for unsteady incompressible viscous flow modeled by Navier-Stokes equations, *Contemporary Mathematics*, Vol. 157, pp. 421-431.

Katta, V.R. and Roquemore, W.M. (1996), Numerical studies on trapped-vortex combustor, *AIAA 96-2660.*

Kelecy, F.J., Griffin, J.W. and Delaney, R.A. (1995), The effect of vane-blade spacing on transonic turbine stage performance, *AGARD-CP-571*, Paper # 5.

Kellogg, S.(2000), Immersed boundary methods with applications to flow control, *M.S. Thesis*, Rice University, TX.

Mancilla, P.C. (2001), Flame stability in a trapped-vortex spray-combustor, *M.S. Thesis*, Louisiana State University, LA.

Peskin, C. S. (1977), Numerical analysis of blood flow in the heart, *J. Comp. Phy.*, Vol. 25, pp. 220-252.

Rai, M.M. and Madavan, N.K. (1990), Multi-airfoil Navier-Stokes simulations of turbine rotor-stator interaction, *J. Turbomachinery*, Vol. 112, pp. 377-384.

Saxer, A.P. and Giles, M.B. (1994), Predictions of three-dimensional steady and unsteady inviscid transonic stator/rotor interaction with inlet radial temperature nonuniformity, *J. Turbomachinery*, Vol. 116, pp. 347-357.

Sharma, O.P., Ni, R.H. and Tanrikut, S. (1994). Unsteady flows in turbines – Impact on design procedure, *AGARD-LS-195*, Paper # 5.

Stone, C. and Menon, S. (2000), Simulation of Fuel-Air Mixing and Combustion in a Trapped-Vortex Combustor, *AIAA Paper No.00-0478*, 38th AIAA Aerospace Sciences Meeting and Exhibit, Reno, NV.

Yusof, J. Mohd. (1996), Interaction of massive particles with turbulence, *Ph.D. Dissertation*, Cornell University.